

Spacecraft energy management using convex optimisation

Martin Doff-Sotta^{a,*}, Mark Cannon^a, James Richard Forbes^b

^a Control Group, University of Oxford, United Kingdom

^b Department of Mechanical Engineering, McGill University, Canada

ARTICLE INFO

Keywords:

Convex optimisation
Energy management
Spacecraft
Model predictive control (MPC)

ABSTRACT

This paper considers a spacecraft energy management strategy for optimally scheduling the power available for secondary tasks, such as communications and scientific payloads, while meeting the power demand for primary tasks, such as thermal management and propulsion, and adhering to operating constraints. A solution based on convex optimisation and model predictive control is proposed. Mathematical models of the various energy subsystems are used to formulate the energy management task over a future horizon as a constrained optimisation problem. We show that this problem can be formulated as a convex program and we derive an energy management strategy in the form of a model predictive control law. The convex problem formulation guarantees global optimality of the presented solution and opens the way for future onboard real-time implementations.

1. Introduction

Autonomous spacecraft rely on algorithms that allow onboard subsystems to make decisions without human intervention. Onboard power systems are required to meet stringent operating constraints, and coordination strategies for the various energy sources, such as solar panels and batteries, are needed. Optimal energy management systems are capable of extending the useful life of spacecraft by improving battery health, as well as reducing launch mass and improving reliability by facilitating the use of electric, hybrid or multimode propulsion systems [1,2]. Moreover, energy management is needed to ensure that the energy stored can continue to meet the power demand despite declining energy storage capacity or unforeseen events and failures [3].

Historically the energy management problem has been addressed by power system analysts who were responsible for validating the command sequence from a ground control station. This task required predicting the load profile and source power availability, checking that operational constraints are not violated and responding to fault conditions [4]. In practice, most of the process was automated and executed with on-ground computers. This approach was expensive in terms of human resources and was prone to round-trip communication delays [5]. It was thus natural to consider transferring the power management task onboard the spacecraft. The Deep Space One New Millennium Program, launched in 1998, is an early example of a mission to use a fully autonomous power management algorithm that includes online command sequence validation [4].

More recently, online management of spacecraft power systems was investigated in [6]. In this setting, each task has several degrees of refinement (versions), requiring varying amounts of power. The power management algorithm attempts to find the optimal version for each task without compromising the energy budget over an orbit. The feasibility and efficiency of braking energy recovery through the use of a flywheel is discussed in [7]. Variable speed control moment gyro are leveraged in [8] in order to eliminate the chemical deterioration factor of the battery for an Earth observation satellite. This is achieved by minimising charge and discharge cycles over an orbit as the spacecraft undergoes successive eclipse and illumination phases, while maintaining proper attitude control. The energy management strategy is obtained by solving a nonlinear multi-objective optimisation problem using a general purpose nonlinear programming solver, which is not suitable for real-time operation due its relatively long computation time. In [9], the energy management optimisation problem for a spacecraft equipped with solar panels and battery is solved with a market management algorithm. Electrical and thermal models are included in the optimisation, which allows to perform model-based optimisation, but no predictive information is included.

The existing literature on spacecraft energy management is largely restricted to heuristic strategies where the energy transfers between the subsystems are planned offline without guarantees of constraint satisfaction, or to nonlinear optimisation approaches that are not computationally tractable for real-time operation. On the other hand, recent research in the context of hybrid electric vehicles [10] and hybrid

* Corresponding author.

E-mail address: martin.doff-sotta@eng.ox.ac.uk (M. Doff-Sotta).

<https://doi.org/10.1016/j.ecmx.2022.100325>

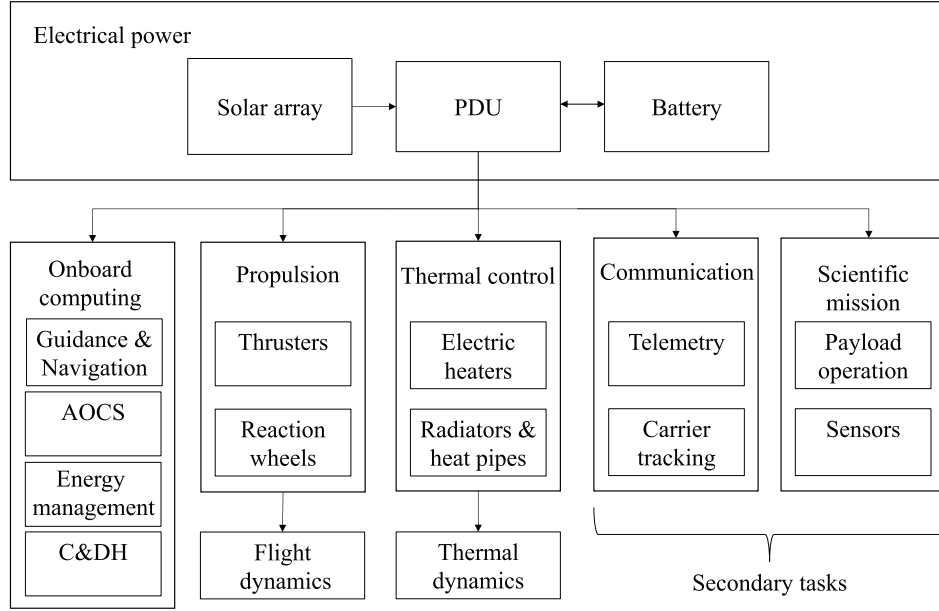


Fig. 1. High-level overview of spacecraft power subsystems, inspired from [18].

aircraft [11,12] has successfully leveraged efficient optimisation strategies to solve similar energy management problems online. These approaches use convex formulations of the optimisation problem and thus exploit advances in convex optimisation. They are also able to ensure robustness to model uncertainty and disturbances [13]. The deployment of real-time MPC-based energy management strategies to new systems is only limited by the ability to formulate the problem as a convex program. However, many optimisation problems that appear computationally intractable at first sight can be reduced to convex problems with lossless manipulations or at the cost of reasonable simplifications that preserve the physics of the process [14]. The robustness guarantees of MPC to model uncertainty then offer some guard against these simplifying assumptions [15].

The objective of the current paper is to show that a computationally tractable optimal energy management strategy can be applied to a comprehensive spacecraft model. We show that mathematical models of the various spacecraft subsystems can be integrated in a convex optimisation that forms the basis of an MPC iteration to be solved online. The outcome is a computationally efficient energy management strategy that optimises some objective online, adapts to unplanned events or uncertainty (such as poorly modeled dynamics) while guaranteeing constraint satisfaction.

We derive the thermal, orbital and rotational dynamics of the spacecraft and the battery, solar panel, electric thrusters and reaction wheels are modelled from first principles. The resulting lumped parameter dynamical models are used to establish an open-loop optimal control problem (OOC), for which we derive a convex formulation under the simplifying assumption that the spacecraft trajectory is prescribed. The solution of this problem predicts the optimal distribution of power among the various components so as to minimise a cost function subject to constraints. In particular, power transfers between the energy subsystems are planned in real time to maximise the execution of secondary tasks, such as the operation of communication hardware or scientific payloads, while guaranteeing enough resources are available to accomplish primary tasks, such as cooling critical systems and maintaining a desired orbit. A case study based on the Eutelsat 172B spacecraft is presented. We use the general purpose convex programming software package CVX [16] with solver Mosek [17] to obtain a solution to the energy management problem, with global optimality guaranteed. The solution can be used as a basis for secondary task

planning as it determines the optimal power availability in real time. We also show that the MPC energy management strategy provides robustness to modelling errors.

The paper is organised as follows. Mathematical models for all energy subsystems are derived in Section 2, along with dynamical and thermal models of the spacecraft. These are used in Section 3 to construct a discrete time energy management problem as a convex OOC. The numerical solution of this problem is then discussed and is used in Section 4 to define a MPC law for a given mission scenario. Conclusions are drawn and extensions are discussed in Section 5.

2. Modelling

We consider a spacecraft equipped with reaction wheels, Hall-effect electric thrusters, solar panels, batteries and other loads. In this section we derive simplified models for the propulsion, electrical and thermal subsystems. We first give an overview of the power architecture.

2.1. Power architecture

The electrical power subsystem consists of a solar panel, battery and power distribution unit (PDU) that arbitrates power flows across the system (Fig. 1). The PDU is commanded by the energy management module that decides how power is allocated to the various subsystems. The onboard computing subsystem is host for all computations executed onboard, including the energy management algorithm, the guidance and navigation module that estimates the state of the spacecraft and computes a trajectory, the attitude and orbit control system (AOCS) whose role is to stabilise the spacecraft dynamics around the computed trajectory, and the command and data handling (C&DH) system that manages data exchanges between subsystems. Control commands from the AOCS are sent to the propulsion subsystem to control the spacecraft dynamics. Electric thrusters are typically used for orbital control and reaction wheels for attitude control. The thermal control subsystem maintains spacecraft components at a suitable operating temperature via heaters and heat pipes conveying heat towards radiators. Secondary tasks include sending data to the ground control station via the communication subsystem, as well as payload operations such as payload deployment and data collection.

The power flows in the system are given by

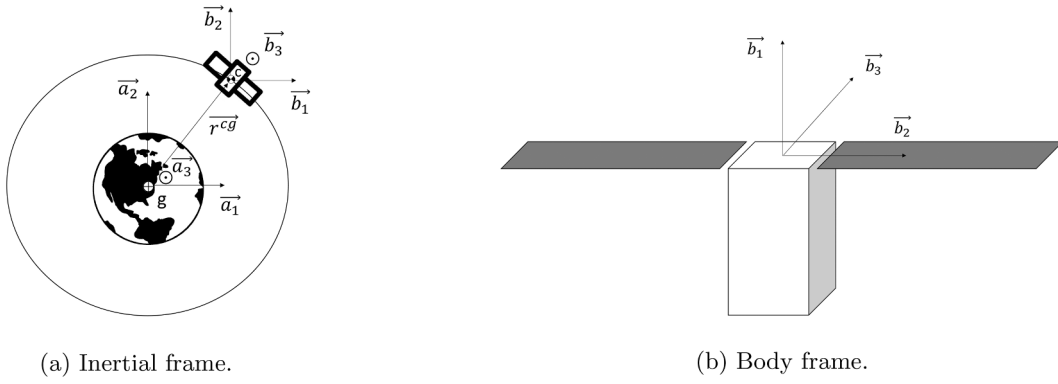


Fig. 2. Spacecraft motion and reference frames.

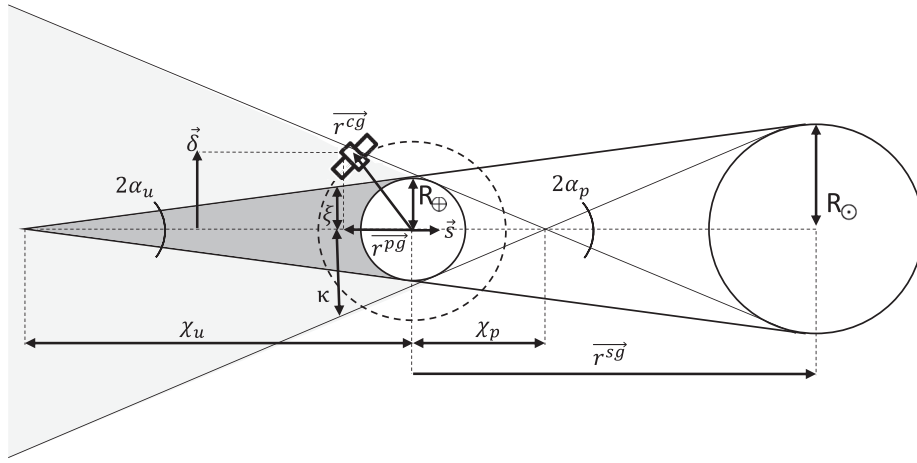


Fig. 3. Umbra (dark-shaded) and penumbra (lightly-shaded) cones.

$$P_s + P_{\text{out}} = P_c + P_a + P_t + P_h + P_l, \quad (1)$$

where P_s is the power generated by the solar array, P_{out} is the power delivered by the battery, P_c is the power consumed by onboard computing, P_a is the power required by the electric motors driving the reaction wheels, P_t is the power required by the electric thrusters, P_h is the power required by the heaters, and P_l is the power available to secondary tasks.

The problem at hand is to maximise the power available to the secondary tasks while satisfying all dynamical, electrical and thermal constraints over a future time interval T . The objective to be minimised is thus

$$J = - \int_0^T P_l dt. \quad (2)$$

We now derive mathematical models for all subsystems of the power architecture.

2.2. Propulsion

2.2.1. Flight dynamics

Consider the spacecraft in a geostationary orbit (GEO) as illustrated in Fig. 2. Let \mathcal{F}_a be an inertial frame fixed to the Earth with basis vectors $\{\vec{a}_1, \vec{a}_2, \vec{a}_3\}$, let \mathcal{F}_b be a body-fixed frame with basis vectors $\{\vec{b}_1, \vec{b}_2, \vec{b}_3\}$, let \mathcal{F}_w be the frame formed with vectors $\{\vec{w}_1, \vec{w}_2, \vec{w}_3\}$ aligned with the reaction wheels' spin axes.

The orbital dynamics resolved in the Earth-fixed frame are given by [19,20]

$$\dot{\mathbf{v}}_a^{cg} = -\mu \frac{\mathbf{r}_a^{cg}}{\|\mathbf{r}_a^{cg}\|^3} + \mathbf{f}_a^{\text{ext}} + \frac{1}{m} \mathbf{C}_{ba}^T \mathbf{f}_b, \quad \mathbf{v}_a^{cg}(0) = \mathbf{v}_{a,0}^{cg}, \quad (3)$$

$$\dot{\mathbf{r}}_a^{cg} = \mathbf{v}_a^{cg}, \quad \mathbf{r}_a^{cg}(0) = \mathbf{r}_{a,0}^{cg}, \quad (4)$$

where \mathbf{r}_a^{cg} is the position of the spacecraft centre of mass c relative to the centre of the Earth g resolved in \mathcal{F}_a , \mathbf{v}_a^{cg} is the velocity of the spacecraft centre of mass c relative to g resolved in \mathcal{F}_a , $\mathbf{f}_a^{\text{ext}}$ are external forces resolved in \mathcal{F}_a , \mathbf{f}_b is the force generated by the electrical thrusters resolved in \mathcal{F}_b , $\mathbf{C}_{ba} \in SO(3)$ is the direction cosine matrix (DCM) from \mathcal{F}_a to \mathcal{F}_b , m is the mass of the spacecraft, $\mu = GM$ is the standard gravitational parameter of the Earth with G the gravitational constant and M the mass of the Earth.

External forces due to magnetic, aerodynamic and meteoroid effects are assumed to be negligible for a GEO orbit [21]. The influence of other celestial bodies is also neglected. Only the external forces due to solar radiation pressure on the solar panel are considered here [19,21]. We start by defining a shadowing parameter modelling the eclipse by the Earth (Fig. 3) following [22]:

$$\nu = \begin{cases} 0, & \text{if } \|\vec{\delta}\| \leq \xi \text{ and } \vec{r}^{cg} \cdot \vec{s} < 0 \\ \frac{\|\vec{\delta}\| - \xi}{\kappa - \xi}, & \text{if } \xi < \|\vec{\delta}\| \leq \kappa \text{ and } \vec{r}^{cg} \cdot \vec{s} < 0 \\ 1, & \text{otherwise,} \end{cases} \quad (5)$$

$$\vec{\delta} = \vec{r}^{cg} - \vec{r}^{pg}, \quad \vec{r}^{pg} = (\vec{r}^{cg} \cdot \vec{s}) \vec{s}, \quad (6)$$

$$\alpha_u = \arcsin\left(\frac{R_\oplus}{\chi_u}\right), \quad \alpha_p = \arcsin\left(\frac{R_\oplus}{\chi_p}\right), \quad (7)$$

$$\chi_u = \frac{R_\oplus}{R_\odot - R_\oplus} AU, \quad \chi_p = \frac{R_\oplus}{R_\odot + R_\oplus} AU, \quad (8)$$

$$\xi = (\chi_u - \|\vec{r}^{pg}\|) \tan \alpha_u, \quad \kappa = (\chi_p + \|\vec{r}^{pg}\|) \tan \alpha_p, \quad (9)$$

where R_\oplus is the radius of the Earth, R_\odot is the radius of the Sun, $AU = \|\vec{r}^{sg}\|$ is the distance from the Earth to the Sun, \vec{r}^{sg} is the ephemeris-dependent position vector between the Sun and the Earth, \vec{r}^{cg} is the position vector between the spacecraft centre of mass and the Earth, \vec{s} is a unit vector aligned along the cone central line, \vec{r}^{pg} is the vector in the opposite direction to \vec{s} with magnitude equal to the projection of \vec{r}^{cg} onto the cone central line, $\vec{\delta}$ is the position of the spacecraft relative to the cone central line, ξ is the umbral cone half basis at the spacecraft projection point and κ is the penumbral cone half basis at the spacecraft projection point. The force due to solar radiation pressure is given by

$$\vec{f}_a^{\text{ext}} = -\nu p A_s \hat{s}_a,$$

where A_s is the surface area of the solar panel, p is the Sun effective pressure on the spacecraft, $\hat{s}_a = (\vec{r}_a^{sg} - \vec{r}_a^{cg}) / \|\vec{r}_a^{sg} - \vec{r}_a^{cg}\|$ is the unit line-of-sight vector from the spacecraft centre of mass to the Sun, resolved in \mathcal{F}_a . For simplicity, we have assumed that 100% of the solar energy is absorbed by the surface of the solar panel (although in practice specular and diffuse reflection are present).

The DCM update is given by the Poisson formula

$$\dot{\vec{C}}_{ba} = -\omega_b^{ba} \times \vec{C}_{ba}, \quad \vec{C}_{ba}(0) = \vec{C}_{ba,0}, \quad (10)$$

where ω_b^{ba} is the angular velocity of the body frame relative to inertial frame and resolved in \mathcal{F}_b , and the skew-symmetric operator $(\cdot)^\times$ expresses the vector product operation as a matrix multiplication.

The attitude dynamics resolved in the body frame are described by [19,21]

$$\begin{aligned} \vec{J}_b \dot{\omega}_b^{ba} + \dot{\vec{h}}_b^{wb} &= -\omega_b^{ba} \times (\vec{J}_b \omega_b^{ba} + \vec{h}_b^{wb}) + \vec{\tau}_b^{\text{ext}} + \vec{\tau}_b, \\ \omega_b^{ba}(0) &= \omega_{b,0}^{ba}, \end{aligned} \quad (11)$$

where $\vec{\tau}_b$ is the torque from electric thrusters resolved in \mathcal{F}_b , $\vec{\tau}_b^{\text{ext}}$ is the external torque contribution arising mainly from solar pressure resolved in \mathcal{F}_b [21], \vec{J}_b is the total moment of inertia of the spacecraft (i.e. carrier and wheels) resolved in \mathcal{F}_b , $\vec{h}_b^{wb} = \vec{J}_b \omega_b^{wb}$ is the vector containing the angular momenta of the wheels about their respective spin axes \mathcal{F}_w and resolved in \mathcal{F}_b , ω_b^{wb} is the vector of wheel angular velocities relative to their respective spin axes \mathcal{F}_w and resolved in \mathcal{F}_b , and \vec{J}_b is the diagonal matrix of the wheels' moments of inertia about their respective spin axes \mathcal{F}_w and resolved in \mathcal{F}_b .

The main source of external torque acting on a GEO spacecraft arises from a solar radiation pressure imbalance about the centre of mass in penumbra (the solar gradient between extreme parts of the spacecraft, equipped with large solar panels, becoming significant in that zone). The external torque acting on the spacecraft is thus given by [19,21]

$$\vec{\tau}_b^{\text{ext}} = -\nu p \oint_{S_w} \vec{r}_b \hat{s}_b (\vec{n}_b^\top \hat{s}_b) dS,$$

where \vec{r}_b is the position of an infinitesimal element of projected surface $(\vec{n}_b^\top \hat{s}_b) dS$ resolved in \mathcal{F}_b , $S_w \approx A_s$ is the wet (lit) surface area and \vec{n}_b is the surface normal at \vec{r}_b resolved in \mathcal{F}_b . The integral can be difficult to evaluate for complex geometries. However, assuming that the solar radiation pressure imbalance mainly occurs along the solar panel span, the Sun radiation pressure can be viewed as a trapezoidal load on the solar

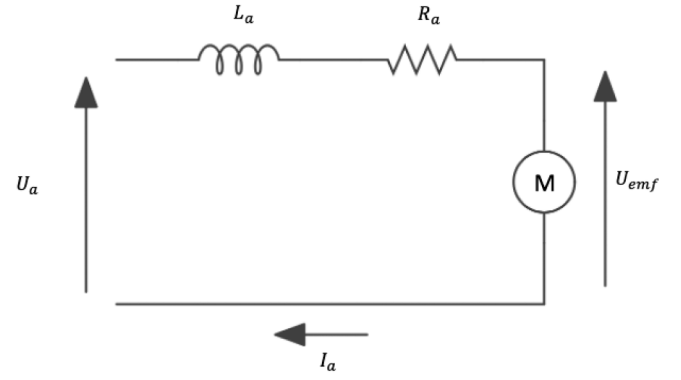


Fig. 4. Equivalent circuit modelling the electric motor.

panel and the torque can be approximated as

$$\tau_b^{\text{ext}} \approx -\Delta_s \frac{l_s^2}{12} b_3$$

where Δ_s is the difference in the force induced by solar radiation across the solar panel span l_s in penumbra.

The dynamics of the reaction wheels are given by [21]

$$\vec{J}_b (\dot{\omega}_b^{ba} + \dot{\omega}_b^{wb}) = \vec{g}_b, \quad \omega_b^{wb}(0) = \omega_{b,0}^{wb} \quad (12)$$

where \vec{g}_b is the vector of torques exerted by the carrier on individual wheels.

2.2.2. Reaction wheels

We assume that each reaction wheel i is actuated by a DC motor, whose equivalent circuit is shown in Fig. 4. Application of Kirchhoff's second law yields [23]

$$U_{a,i} = L_a \frac{dI_{a,i}}{dt} + R_a I_{a,i} + U_{\text{emf},i},$$

where $U_{a,i}$ is the armature voltage, $I_{a,i}$ the armature current, R_a the armature resistance, L_a the armature inductance, $U_{\text{emf},i} = k_w \omega_{b,i}^{wb}$ the back emf proportional to the wheel rotation speed ($\omega_{b,i}^{wb}$ is the angular velocity of wheel i about its spin axis). The torque generated is proportional to the armature current

$$g_{b,i} = k_a I_{a,i}.$$

In the stationary regime, the voltage equation reduces to

$$U_{a,i} = \frac{R_a}{k_a} g_{b,i} + k_w \omega_{b,i}^{wb},$$

and the power equation can be obtained by multiplying both sides by $I_{a,i}$ as follows

$$P_{a,i} = \frac{R_a}{k_a^2} g_{b,i}^2 + \frac{k_w}{k_a} \omega_{b,i}^{wb} g_{b,i},$$

where $P_{a,i} = U_{a,i} I_{a,i}$ is the input electric power. Generalising the result for all motors yields

$$P_a = \frac{R_a}{k_a^2} \|\vec{g}_b\|^2 + \frac{k_w}{k_a} \vec{g}_b^\top \vec{\omega}_b^{wb}, \quad (13)$$

where P_a is the total input power to the motors. We assume elementwise bounds on the motor torque and angular velocity vectors:

$$\vec{g} \leq \vec{g}_b \leq \vec{g}, \quad (14)$$

$$\vec{\omega} \leq \vec{\omega}_b^{wb} \leq \vec{\omega}. \quad (15)$$

2.2.3. Thrusters

The thrust magnitude $T_{\text{HET},i}$ produced by the i th thruster is a function of the ion beam current $I_{\text{HET},i}$ and (constant) voltage V_{HET} through which ions are accelerated as follows [24]

$$T_{\text{HET},i} = \eta_{\text{HET}} \sqrt{\frac{2MV_{\text{HET}}}{q}} I_{\text{HET},i},$$

where M is the atomic mass of the ion, q is the charge and η_{HET} accounts for losses due to, for example, electron collisions, magnetic field generation, deflection of the beam and cathode heater operation. Since $P_{\text{HET},i} = V_{\text{HET}} I_{\text{HET},i}$ where $P_{\text{HET},i}$ is the input power to the thruster, we obtain

$$T_{\text{HET},i} = \eta_{\text{HET}} \sqrt{\frac{2M}{qV_{\text{HET}}}} P_{\text{HET},i},$$

and assume the following limits on power

$$\underline{P}_{\text{HET}} \leq P_{\text{HET},i} \leq \bar{P}_{\text{HET}}, \quad \forall i \in \{1, \dots, N_{\text{HET}}\}, \quad (16)$$

where

$$\underline{P}_{\text{HET}} = \frac{1}{\eta_{\text{HET}}} \sqrt{\frac{qV_{\text{HET}}}{2M}} T_{\text{HET}},$$

$$\bar{P}_{\text{HET}} = \frac{1}{\eta_{\text{HET}}} \sqrt{\frac{qV_{\text{HET}}}{2M}} \bar{T}_{\text{HET}}.$$

Considering N_{HET} thrusters, and assuming for simplicity that thrust forces are aligned with the centre of mass so that no torques are generated, the following equation relates the power contribution from each thruster to forces f_b acting on the spacecraft

$$f_b = \Theta \eta_{\text{HET}} \sqrt{\frac{2M}{qV_{\text{HET}}}} P_{\text{HET}},$$

where $P_{\text{HET}} = [P_{\text{HET},1} \ P_{\text{HET},2} \ \dots \ P_{\text{HET},N_{\text{HET}}}]^T$ is the vector of thruster powers, Θ is a matrix depending on the geometrical configuration of the thrusters. We denote the total power supplied to the thrusters as

$$P_t = I^T P_{\text{HET}}. \quad (17)$$

2.2.4. Control

The AOCS algorithms ensure stabilisation of the spacecraft attitude and orbit around a desired trajectory.

Considering a telecommunication mission scenario, the desired attitude is such that the spacecraft achieves Earth pointing. Defining the desired attitude frame \mathcal{F}_d , the error DCM between the attitude of the body C_{ba} and desired attitude C_{da} can be expressed as

$$C_{bd} = C_{ba} C_{da}^T.$$

The desired attitude is then achieved by generating angular momenta with the reaction wheels. The $SO(3)$ -preserving control law for the reaction wheel torques is [25]

$$g_b = k_o \omega_b^{ba} - k \frac{1}{2} (C_{bd} - C_{bd}^T)^\wedge, \quad (18)$$

where k, k_o are gains and $(\cdot)^\wedge$ represents the “uncross” operator defined by $(v^\times)^\wedge = v$.

The objective of orbital control is to maintain the spacecraft along a geostationary orbit. In the presence of external disturbances, corrections are required from the thrusters to keep the spacecraft on the desired orbit r_d^{cg} . We assume for simplicity that the thrust forces generated are aligned with the centre of mass of the vehicle, so that the thrusters only

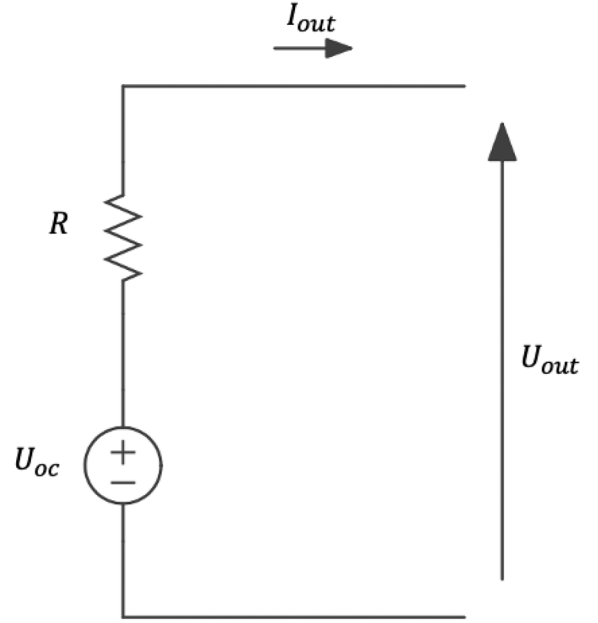


Fig. 5. Equivalent circuit modelling the battery.

affect translational motion. This allows us to decouple the orbital and attitude control problems. A simple PD controller is used [25]

$$f_b = m C_{ba} (k_p (C_{da}^T r_d^{cg} - r_a^{cg}) + k_d (C_{da}^T \dot{r}_d^{cg} - \dot{r}_a^{cg})), \quad (19)$$

and, since the thrusters generate no torques in our scenario, we necessarily have

$$\tau_b = 0. \quad (20)$$

2.3. Electrical power

2.3.1. Battery

The battery is modelled as an open circuit voltage source U_{oc} in series with an internal resistor R [11,23] as illustrated by the equivalent circuit in Fig. 5, assuming no dependence of these variables on state of charge, temperature and ageing, and ignoring electrode capacitance.

According to Kirchhoff's second law

$$U_{out} = U_{oc} - R I_{out},$$

where U_{out} is the battery voltage at the output and I_{out} the battery current. Letting $P_{out} = U_{out} I_{out}$, the associated power balance can be written as

$$P_{out} = U_{oc} I_{out} - R I_{out}^2,$$

Solving for I_{out} yields

$$I_{out} = \frac{U_{oc}}{2R} - \sqrt{\frac{U_{oc}^2}{4R^2} - \frac{P_{out}}{R}}.$$

Multiplying both sides of this equation by U_{oc} and rearranging yields

$$P_b = g \left(P_{out} \right) = \frac{U_{oc}^2}{2R} \left(1 - \sqrt{1 - \frac{4R}{U_{oc}^2} P_{out}} \right), \quad (21)$$

where $P_b = U_{oc} I_{out}$ and $g(\cdot)$ defines the input–output map.

The evolution of the energy stored in the battery E is given by the following update equation [11]

$$\dot{E} = -\gamma P_b, \quad (22)$$

where

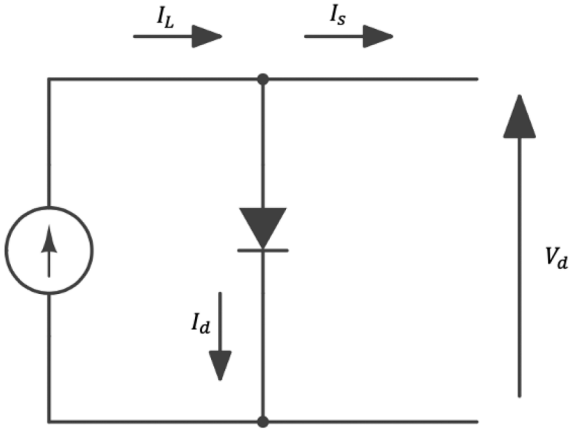


Fig. 6. Equivalent circuit modelling the solar panel.

$$\gamma = \begin{cases} 1, & \text{if } I_{\text{out}} > 0, \\ \eta_b < 1, & \text{otherwise,} \end{cases}$$

in order to account for losses during charging. The energy stored in the battery must satisfy the constraint

$$\underline{E} \leq E \leq \bar{E}. \quad (23)$$

Finally the power delivered by the battery satisfies [26]

$$P_{\text{out}} \leq \frac{U_{\text{oc}}^2}{4R}. \quad (24)$$

Battery packs typically consist of rectangular arrays of N_{b_p} parallel sets of N_{b_s} interconnected cells in series. The open-circuit voltage U_{oc} and internal resistance R of the whole pack are given as a function of the cell open-circuit voltage U_{oc}^c and cell internal resistance R^c as follows

$$U_{\text{oc}} = N_{b_s} U_{\text{oc}}^c, \quad R = \frac{N_{b_s}}{N_{b_p}} R^c.$$

2.3.2. Solar array

Consider the ideal single-diode photovoltaic (PV) model in Fig. 6.

The simplified equivalent circuit consists of a current source in parallel with an ideal diode [27]. We assume no leakages to ground and no series losses. The relationship between the diode current I_d and voltage V_d is given by

$$I_d = I_{ds} \left(e^{\frac{V_d}{V_t}} - 1 \right),$$

where I_{ds} is the saturation current

$$I_{ds} = I_{sc} e^{-\frac{V_{\text{oc}}}{V_t}}. \quad (25)$$

The open circuit voltage V_{oc} , thermal voltage V_t , and short circuit current I_{sc} depend on the temperature of the cell. Since solar panels are assembled by interconnecting N_p parallel sets of N_s cells in series, the following relations exist between the parameters for the cells and the whole panel [28]

$$I_{sc} = N_p I_{sc}^c, \quad I_L = N_p I_L^c, \\ V_t = N_s V_t^c, \quad V_d = N_s V_d^c, \quad V_{\text{oc}} = N_s V_{\text{oc}}^c.$$

Applying Kirchhoff's first law to the circuit in Fig. 6 yields the current I_s at the output of the cell

$$I_s = I_L - I_d = I_L - I_{ds} \left(e^{\frac{V_d}{V_t}} - 1 \right)$$

where I_L is the current due to irradiation, given by

$$I_L = \frac{\nu I_0 G_0 R_{\odot}^2}{\|r_a^{\text{sg}} - r_a^{\text{cg}}\|^2} |\cos \phi_s|. \quad (26)$$

Here I_0 is a calibration parameter obtained by measuring I_L in known solar irradiation conditions, G_0 the intensity of solar radiation at the surface of the Sun, ϕ_s is the angle between the solar panel normal and the Sun, ν is the shadowing factor modelling the eclipse by the Earth as illustrated in Fig. 3. The power P_s produced by the solar panel is given by

$$P_s = V_d (I_L - I_{ds} (e^{V_d/V_t} - 1)) \eta_s \quad (27)$$

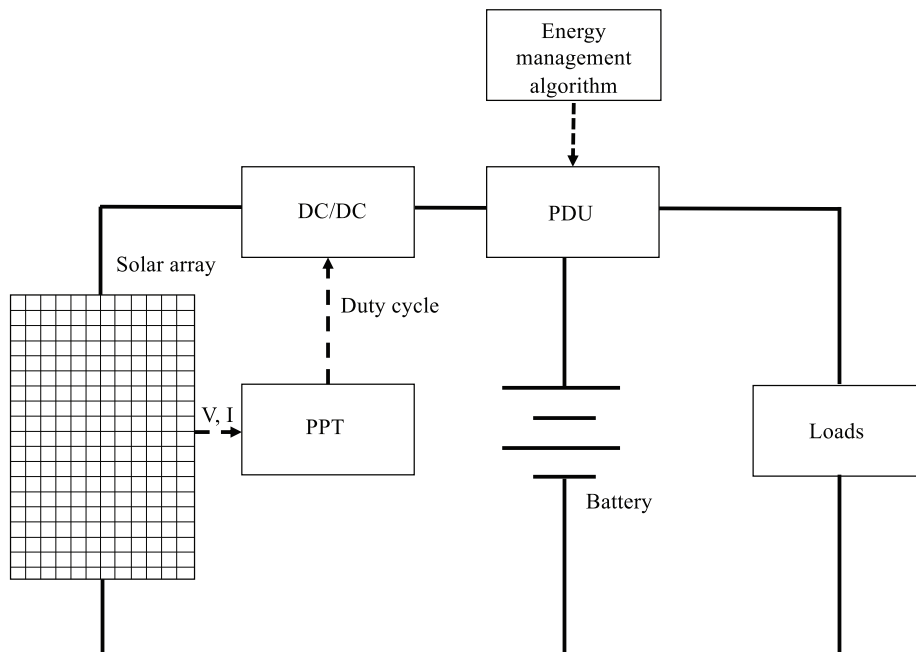


Fig. 7. PPT architecture.

where η_s is an efficiency accounting, for example, for losses due to cell mismatch, parameter calibration and micrometeoroid effects.

As illustrated in Fig. 7, the PV array is connected to a DC/DC converter used as a power point tracker (PPT) that sets the PV array voltage V_d at its maximum power point so as to maximise P_s while matching the converter output voltage with the required bus voltage. The extremum is found by solving the following equation for V_d

$$\frac{dP_s}{dV_d} = 0 \Leftrightarrow I_L + I_{ds} - I_{ds} e^{V_d/V_t} \left(1 + V_d/V_t \right) = 0.$$

Since V_d/V_t is a non-negative real number, the solution is obtained in terms of the Lambert W function,

$$V_d = V_t \left(W_0 \left(\frac{I_L + I_{ds}}{I_{ds}} e \right) - 1 \right), \quad (28)$$

where W_0 is the principal branch of W , defined for any real scalar $x \geq 0$ as follows [29]

$$x = W_0(x) e^{W_0(x)}.$$

The function $W_0(x)$ can be approximated to within 0.2% maximum relative error for $x > 3 \times 10^{-5}$ using

$$W_0(x) \approx (1 + \vartheta) \ln \left(\frac{\frac{6}{5}x}{\ln \left(\frac{\frac{12}{5}x}{\ln \left(1 + \frac{12}{5}x \right)} \right)} \right) - \vartheta \ln \left(\frac{2x}{\ln(1 + 2x)} \right),$$

with $\vartheta = 0.4586887$ [30].

2.3.3. Power distribution unit

A PDU is used (as shown in Fig. 1)) to regulate and distribute voltage to the various loads as they typically operate at different voltage levels. Fuses are also implemented to protect the power system from faults in the load circuits. For simplicity, we assume that the efficiency of power conversion is 100%.

2.4. Onboard computing

Onboard computing tasks include the operation of the micro-controllers running the control, state estimation and energy management algorithms, the command and data handling unit, along with the active sensors used to estimate the state of the spacecraft. We account for the total power consumption from onboard computing by a constant term $P_c = 1.75 \text{ kW}$ in the power balance, namely $\sim 5\%$ of the total power budget [18].

2.5. Thermal control

We limit our analysis to active temperature regulation of sensitive electronic components in the onboard computing subsystem and to solar panels with temperature-dependent cell parameters. Although in practice other components could be considered for thermal regulation, most of these could either be regulated passively (through proper design, insulation or the use of special coating) or be regulated actively using similar thermal models.

2.5.1. Onboard computing thermal model

The onboard computing subsystem can be modelled thermally as a box with thermal capacitance C_c . We assume that 100% of the power P_c consumed by the onboard computing subsystem is converted into internal heat within this box. Outgoing heat flows are due to conductive transfers through the spacecraft armature. We ignore radiative transfers and assume that the box is protected by multi-layer insulation. A thermal control system is used to maintain the temperature of the electronics inside the box at suitable levels at the beginning of the mission and during eclipses. Active thermal control is achieved with an electric

heater that supplies heat P_h to the system. Passive cooling is achieved by conduction with a heat pipe transferring heat to a radiator. The working fluid is ammonia in a saturated vapour phase and at temperature T_f . The thermal dynamics describing the evolution of the onboard computing electronics temperature T_c are given by [31]

$$C_c \dot{T}_c = P_c + P_h - G_f (T_c - T_f) - G_b (T_c - T_b), \quad (29)$$

$$T_c(0) = T_{c,0}, \quad \underline{T}_c \leq T_c \leq \overline{T}_c, \quad (30)$$

where T_b is the temperature at the surface of the spacecraft, $G_b = k_b S_b / d$ is the thermal conductance between the electronics casing and the spacecraft armature (k_b, S_b, d are respectively the thermal conductivity, contact surface, and length of the conduction path between the electronics casing and the spacecraft armature), $G_f = k_f S_f / t$ is the thermal conductance between the electronics casing and the heat pipe (k_f, S_f, t are respectively the thermal conductivity, contact surface and thickness between the heat pipe and the electronics casing). The electric heater operation is limited by

$$0 \leq P_h \leq \overline{P}_h, \quad (31)$$

The rate of change of the temperature at the surface of the spacecraft is determined by incident radiation, heat from electronic components transferred by conduction and outgoing radiation [31]

$$C_b \dot{T}_b = Q_b + G_b (T_c - T_b) - \epsilon_b A_b \sigma T_b^4, \quad (32)$$

$$T_b(0) = T_{b,0}, \quad \underline{T}_b \leq T_b \leq \overline{T}_b, \quad (33)$$

where C_b is the thermal capacitance of the spacecraft surface, ϵ_b is the infrared emissivity of the spacecraft surface, σ is the Stefan–Boltzmann constant, A_b is the area of the spacecraft surface directly exposed to sunlight, Q_b is the heat due to incident radiation from the Sun. Neglecting albedo effect and heat due to planetary infrared radiation for a GEO mission [18], and assuming for simplicity that the body is spherical, the solar heat is given by

$$Q_b = \frac{\gamma_b A_b G_0 R_\odot^2}{\| \mathbf{r}_a^{\text{sg}} - \mathbf{r}_a^{\text{cg}} \|^2}, \quad (34)$$

where γ_b is the solar absorptance of the surface.

Together, Eqs. (29)–(34) drive the coupled evolution of the onboard computing subsystem and external surface temperatures.

2.5.2. Solar panel thermal model

The PV panel open circuit voltage V_{oc} , short circuit current I_{sc} and thermal voltage V_t depend on the temperature T_s at the panel surface via

$$V_{oc}(T_s) = V_{oc}(T_0) + \alpha_{V_{oc}} (T_s - T_0), \quad (35)$$

$$I_{sc}(T_s) = I_{sc}(T_0) + \beta_{I_{sc}} (T_s - T_0), \quad (36)$$

$$V_t = k_B T_s / q_e, \quad (37)$$

where T_0 is a reference temperature at which the parameters are measured, $\alpha_{V_{oc}}, \beta_{I_{sc}}$ describe the change of voltage and current with temperature, k_B is the Boltzmann constant and q_e is the electric charge of an electron. The saturation current of the PV panel depends on these parameters and should thus be updated accordingly.

The evolution of the temperature T_s at the PV panel surface is given by the thermal energy balance [31]

$$C_s \dot{T}_s = Q_s - \epsilon_s A_s \sigma T_s^4, \quad (38)$$

$$T_s(0) = T_{s,0}, \quad \underline{T}_s \leq T_s \leq \overline{T}_s, \quad (39)$$

where C_s is the thermal capacitance of the PV panel, ϵ_s is the infrared

emissivity of the PV panel surface, A_s is the area of the PV panel surface, and Q_s is the heat due to incident radiation from the Sun, defined by

$$Q_s = \frac{\nu \gamma_s A_s G_0 R_\odot^2}{\|r_a^{sg} - r_s^{sg}\|^2} |\cos \phi_s|, \quad (40)$$

where γ_s is the solar absorptance of the solar array surface.

2.6. Model-based optimisation

An optimisation problem based directly on (1)-(40) would be non-convex, making a real-time implementation of an energy management algorithm that relies on its solution computationally intractable. Indeed, the dynamics of the vehicle are nonlinear, the reaction wheel power involves quadratic losses in the reaction wheel torque, the input–output map between the battery internal power and output power is nonlinear, the charging–discharging efficiency of the battery is nonlinear, the solar panel parameters are temperature dependent, the thermal dynamics are nonlinear, solar radiation is nonlinearly coupled with the spacecraft position etc. In the next section we therefore present a series of assumptions that allows us to derive a convex formulation of an energy management problem that is suitable for an online implementation.

3. Energy management

Using the models described in Section 2, we introduce a discrete-time convex optimisation problem which is the basis of a model predictive control law implementing an optimal energy management strategy for the spacecraft. We first show that, under mild assumptions, the problem can be reduced to a convex program which is suitable for real-time embedded control.

3.1. Convex formulation

A convex problem formulation allows the use of convex solvers that are guaranteed to converge to globally optimal solutions whenever the problem is feasible. Convex programs are of the form

$$\begin{aligned} \min_{\theta} \quad & f_0(\theta) \\ \text{s.t.} \quad & f_i(\theta) = 0, \quad i = 1, \dots, m \\ & g_j(\theta) \leq 0, \quad j = 1, \dots, l \end{aligned}$$

with f_0 convex, f_i linear and g_j convex with respect to the optimisation variable θ .

In order to derive a convex formulation of the energy management problem, we make the following assumptions on the models developed in Section 2.

3.1.1. Prescribed trajectories

The motion is prescribed (i.e. $r_a^{cg}, \omega_b^{ba}, \omega_b^{wb}, C_{ba}$ can be computed *a priori*). Consequently, the forces and torques f_b, τ_b, g_b are also prescribed, along with all phenomena depending on the position of the spacecraft such as solar radiation force and momentum, solar radiation heat, eclipses, etc. The position of the Earth relative to the Sun is assumed constant for simplicity.

3.1.2. Battery input–output map relaxation

Noting that the battery input–output map $g(\cdot)$ in Eq. (21) is a convex function of P_{out} , we relax the equality in (21) as follows

$$P_b \geq g(P_{out}) = \frac{U_{oc}^2}{2R} \left(1 - \sqrt{1 - \frac{4R}{U_{oc}^2} P_{out}} \right). \quad (41)$$

This inequality is indeed necessarily satisfied with equality at the optimum, since otherwise there exists $\delta > 0$ such that

$$P_b = g(P_{out}) + \delta,$$

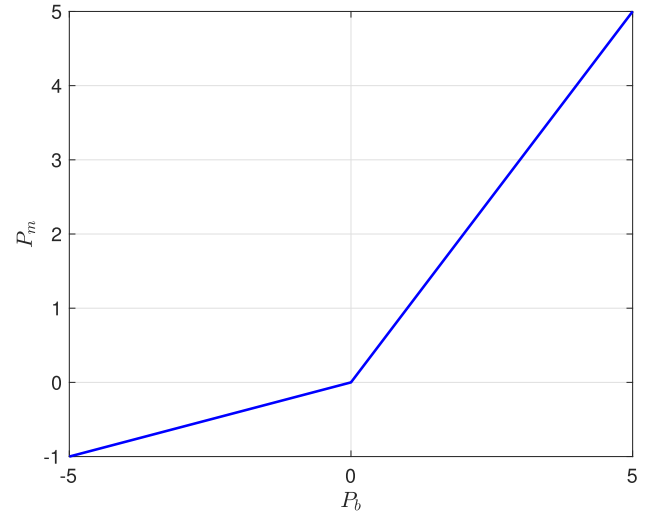


Fig. 8. The convex constraint (42) for the case that $\eta = 0.2$.

which would mean that some internal power of the battery is wasted in producing power δ . The implied solution would not be optimal since this power could either be supplied to increase the power available to secondary tasks, or saved for latter use.

3.1.3. Battery efficiency reformulation

The battery efficiency γ in Eq. (22) is dependent on the sign of the battery current (charging the battery being less efficient than discharging), which introduces a nonlinear equality constraint in the problem. In order to obtain a convex formulation of the energy update equality, we introduce a new variable P_m and set

$$P_m \geq \max\{P_b, \eta_b P_b\}, \quad (42)$$

$$\dot{E} = -P_m. \quad (43)$$

The constraint (42) is convex whenever $\eta \leq 1$ (Fig. 8). Furthermore, by reasoning similar to the argument given for the battery input–output map relaxation, it is necessarily active at the optimum.

3.1.4. Prescribed solar array temperature

Since orbital motion is prescribed, the heats Q_b and Q_s in Eqs. (34) and (40) can be computed *a priori*. It is thus possible to predict the solar array temperature *a priori* via (38) and remove T_s from the optimisation. The inequality constraints on T_s are enforced by design.

The temperature-dependent parameters of the solar panel in (35)–(37) can also be computed *a priori*, and thus P_s in (27) can be entirely computed offline.

Note that these predictions can be further refined by taking a series of temperature measurements during commissioning of the spacecraft to improve the model accuracy.

3.1.5. Prescribed external surface temperature

Since the bounds imposed on the electronics temperature are relatively tight, we can approximate T_c in (32) by $T_c \approx \frac{\bar{T}_c + T_c}{2}$ and compute T_b offline so that it is no longer an optimisation variable. The inequality constraints can be satisfied by passive thermal control at the design stage: selection of the proper material, coating, paint, insulation, etc. Again, these predictions can be validated by temperature measurements during commissioning.

3.1.6. Electronics temperature reformulation

The electronics temperature equation can be solved analytically for T_c as follows

$$T_c = a(t)(P_c + P_h + G_b T_b + G_f T_f) + b(t), \quad (44)$$

with

$$a = \frac{1}{G_b + G_f} \left(1 - e^{-\left(\frac{G_b + G_f}{c_c}\right)t} \right), \quad (45)$$

$$b = T_{c,0} e^{-\left(\frac{G_b + G_f}{c_c}\right)t}. \quad (46)$$

3.2. Open-loop optimal control problem

Using discrete-time versions of the spacecraft subsystem models, we now formulate an open-loop optimal control problem (OOC) for computing the optimal power allocation as a finite-dimensional optimisation problem. The solution to this problem is an open-loop strategy that maximises the power available to secondary tasks while satisfying constraints on all subsystems over a future prediction horizon. We use this to define a feedback control strategy by repeatedly solving the OOC at the sampling times $0, \delta, 2\delta, \dots$, where δ is a fixed sampling interval, using information on the current state of all relevant subsystems. By implementing only the first sample of the OOC solution at each sampling instant, we thus obtain a model predictive control (MPC) energy management strategy that is approximately optimal while providing the robustness benefits of feedback control [15].

At the k th sampling instant, we require information on the energy stored in the battery $E(k\delta)$, spacecraft position $\mathbf{r}_a^{\text{cg}}(k\delta)$, velocity $\mathbf{v}_a^{\text{cg}}(k\delta)$, angular velocity $\omega_b^{\text{ba}}(k\delta)$ and attitude $C_{ba}(k\delta)$, angular velocity of reaction wheels $\omega_b^{\text{wb}}(k\delta)$, solar panel temperature $T_s(k\delta)$, external surface temperature $T_b(k\delta)$ and electronics temperature $T_c(k\delta)$. We denote $E_0 = E(k\delta)$, $\mathbf{r}_{a,0}^{\text{cg}} = \mathbf{r}_a^{\text{cg}}(k\delta)$, $\mathbf{v}_{a,0}^{\text{cg}} = \mathbf{v}_a^{\text{cg}}(k\delta)$, $\omega_{b,0}^{\text{ba}} = \omega_b^{\text{ba}}(k\delta)$, $C_{ba,0} = C_{ba}(k\delta)$, $\omega_{b,0}^{\text{wb}} = \omega_b^{\text{wb}}(k\delta)$, $T_{s,0} = T_s(k\delta)$, $T_{b,0} = T_b(k\delta)$, and $T_{c,0} = T_c(k\delta)$ at any time $k\delta$. The notation $\{x_0, x_1, \dots, x_{N-1}\}$ is used for the sequence of current and future values of a variable x predicted at the k th discrete-time step, so that x_i denotes the predicted value of $x((k+i)\delta)$. The prediction horizon is $T = N\delta$, where N is chosen, for example, so that T is at least one orbital period. Applying the proposed modifications in Section 3.1 and using Euler's method to discretise the prediction horizon we obtain a convex, and hence tractable OOC.

Firstly, the variables that were eliminated from the optimisation problem are computed over the prediction horizon, $\forall i \in \{0, \dots, N-1\}$:

$$\mathbf{r}_{a,i}^{\text{cg}} = \mathbf{r}_{a,i-1}^{\text{cg}} + \delta \mathbf{v}_{a,i-1}^{\text{cg}}, \quad (47)$$

$$\mathbf{v}_{a,i}^{\text{cg}} = \mathbf{v}_{a,i-1}^{\text{cg}} - \delta \mu \frac{\mathbf{r}_{a,i-1}^{\text{cg}}}{\|\mathbf{r}_{a,i-1}^{\text{cg}}\|^3} - \delta \nu_{i-1} p A_s \hat{\mathbf{s}}_{a,i-1} + \delta \frac{1}{m} \mathbf{C}_{ba,i-1}^\top \mathbf{f}_{b,i-1}, \quad (48)$$

$$\begin{aligned} \mathbf{J}_b \omega_{b,i}^{\text{ba}} + \bar{\mathbf{J}}_b \omega_{b,i}^{\text{wb}} &= \mathbf{J}_b \omega_{b,i-1}^{\text{ba}} + \bar{\mathbf{J}}_b \omega_{b,i-1}^{\text{wb}} - \delta \omega_{b,i-1}^{\text{ba}} \times \left(\mathbf{J}_b \omega_{b,i-1}^{\text{ba}} + \bar{\mathbf{J}}_b \omega_{b,i-1}^{\text{wb}} \right) \\ &\quad - \delta \Delta_{s,i-1} \frac{I_s^2}{12} \mathbf{b}_3, \end{aligned} \quad (49)$$

$$\mathbf{C}_{ba,i} = e^{-\Psi_{i-1}^\times} \mathbf{C}_{ba,i-1}, \quad \Psi_i = \delta \omega_{b,i}^{\text{ba}}, \quad (50)$$

$$e^{-\Psi_i^\times} = \cos \Psi_i \mathbf{I} + (1 - \cos \Psi_i) \hat{\Psi}_i \hat{\Psi}_i^\top - \sin \Psi_i \hat{\Psi}_i^\times, \quad (51)$$

$$\Psi_i = \sqrt{\Psi_i^\top \Psi_i}, \quad \hat{\Psi}_i = \Psi_i / \Psi_i, \quad (52)$$

$$\bar{\mathbf{J}}_b \left(\omega_{b,i}^{\text{ba}} + \omega_{b,i}^{\text{wb}} \right) = \bar{\mathbf{J}}_b \left(\omega_{b,i-1}^{\text{ba}} + \omega_{b,i-1}^{\text{wb}} \right) + \delta \mathbf{g}_{b,i-1}, \quad (53)$$

$$\mathbf{e}_{a,i} = \mathbf{C}_{da,i}^\top \mathbf{r}_{d,i}^{\text{cg}} - \mathbf{r}_{a,i}^{\text{cg}}, \quad \mathbf{C}_{bd,i} = \mathbf{C}_{ba,i} \mathbf{C}_{da,i}^\top, \quad (54)$$

$$\mathbf{f}_{b,i-1} = m \mathbf{C}_{ba,i-1} (k_p \mathbf{e}_{a,i-1} + k_d (\mathbf{e}_{a,i} - \mathbf{e}_{a,i-1}) / \delta), \quad (55)$$

$$\mathbf{g}_{b,i} = k_w \omega_{b,i}^{\text{ba}} - k \frac{1}{2} \left(\mathbf{C}_{bd,i} - \mathbf{C}_{bd,i}^\top \right)^\wedge, \quad (56)$$

$$\nu_i = \begin{cases} 0, & \text{if } \|\vec{\delta}_i\| \leq \xi_i \text{ and } \vec{r}_i^{\text{cg}} \cdot \vec{s}_i < 0 \\ \frac{\|\vec{\delta}_i\| - \xi_i}{\kappa_i - \xi_i}, & \text{if } \xi_i < \|\vec{\delta}_i\| \leq \kappa_i \text{ and } \vec{r}_i^{\text{cg}} \cdot \vec{s}_i < 0 \\ 1, & \text{otherwise,} \end{cases} \quad (57)$$

$$\vec{\delta}_i = \vec{r}_i^{\text{cg}} - \vec{r}_i^{\text{pg}}, \quad \vec{r}_i^{\text{pg}} = \left(\vec{r}_i^{\text{cg}} \cdot \vec{s}_i \right) \vec{s}_i, \quad (58)$$

$$\alpha_u = \arcsin \frac{R_\oplus}{\chi_u}, \quad \alpha_p = \arcsin \frac{R_\oplus}{\chi_p}, \quad (59)$$

$$\chi_u = \frac{R_\oplus}{R_\odot - R_\oplus} AU, \quad \chi_p = \frac{R_\oplus}{R_\odot + R_\oplus} AU, \quad (60)$$

$$\xi_i = (\chi_u - \|\vec{r}_i^{\text{pg}}\|) \tan \alpha_u, \quad \kappa_i = (\chi_p + \|\vec{r}_i^{\text{pg}}\|) \tan \alpha_p, \quad (61)$$

$$P_{a,i} = \frac{R_a}{k_a^2} \left\| \mathbf{g}_{b,i} \right\|^2 + \frac{k_w}{k_a} \mathbf{g}_{b,i}^\top \omega_{b,i}^{\text{wb}}, \quad (62)$$

$$P_{t,i} = \mathbf{I}^\top \mathbf{P}_{\text{HET},i}, \quad \mathbf{f}_{b,i} = \Theta \eta_{\text{HET}} \sqrt{\frac{2M}{qV_{\text{HET}}}} \mathbf{P}_{\text{HET},i}, \quad (63)$$

$$P_{s,i} = \eta_s V_{d,i} (I_{L,i} - I_{ds,i} (e^{q_e V_{d,i} / (k_B T_{s,i})} - 1)), \quad (64)$$

$$V_{d,i} = \frac{k_B T_{s,i}}{q_e} \left(W_0 \left(\frac{I_{L,i} + I_{ds,i}}{I_{ds,i}} e \right) - 1 \right), \quad (65)$$

$$I_{ds,i} = \left(I_{sc0} + \beta_{sc} \left(T_{s,i} - T_0 \right) \right) e^{-\frac{q_e (V_{oc0} + a_{Voc} (T_{s,i} - T_0))}{k_B T_{s,i}}}, \quad (66)$$

$$I_{L,i} = \frac{\nu_i I_0 G_0 R_\odot^2}{\|\mathbf{r}_{a,i}^{\text{cg}} - \mathbf{r}_{a,i}^{\text{cg}}\|^2} |\cos \phi_{s,i}|, \quad (67)$$

$$\begin{aligned} C_b T_{b,i} &= C_b T_{b,i-1} + \delta \frac{\nu_{i-1} \gamma_b A_b G_0 R_\odot^2}{\|\mathbf{r}_{a,i-1}^{\text{cg}} - \mathbf{r}_{a,i-1}^{\text{cg}}\|^2} |\cos \phi_{s,i-1}| + \delta G_b \left(\frac{T_c + T_c}{2} \right. \\ &\quad \left. - T_{b,i-1} \right) - \delta \epsilon_b A_b \sigma T_{b,i-1}^4, \end{aligned} \quad (68)$$

$$C_s T_{s,i} = C_s T_{s,i-1} + \delta \frac{\nu_{i-1} \gamma_b A_b G_0 R_\odot^2}{\|\mathbf{r}_{a,i-1}^{\text{cg}} - \mathbf{r}_{a,i-1}^{\text{cg}}\|^2} |\cos \phi_{s,i-1}| - \delta \epsilon_s A_s \sigma T_{s,i-1}^4, \quad (69)$$

$$a_i = \frac{1}{G_b + G_f} \left(1 - e^{-\left(\frac{G_b + G_f}{c_c}\right)\delta(k+i)} \right), \quad (70)$$

$$b_i = T_{c,0} e^{-\left(\frac{G_b + G_f}{c_c}\right)\delta(k+i)}, \quad (71)$$

$$\underline{P}_{\text{HET}} \leq P_{\text{HET},i} \leq \bar{P}_{\text{HET}}, \quad (72)$$

$$\underline{\mathbf{g}} \leq \mathbf{g}_{b,i} \leq \bar{\mathbf{g}}, \quad \underline{\omega} \leq \omega_{b,i}^{\text{wb}} \leq \bar{\omega}, \quad (73)$$

$$\underline{T_b} \leq T_{b,i} \leq \bar{T_b}, \quad \underline{T_s} \leq T_{s,i} \leq \bar{T_s}, \quad (74)$$

where $\mathbf{r}_{d,i}^{\text{cg}}$ and $\mathbf{C}_{da,i}$ denote the desired trajectories and Rodrigues' rotation formula is used to update the DCM. The OOC is defined by the following convex program in decision variables $\theta = (P_{\text{out}}, E, T_c, P_m, P_b, P_h, P_l)$,

$$\begin{aligned}
& \min_{P_{\text{out}}, E, T_c, P_m, P_b, P_h, P_l} - \sum_{i=0}^{N-1} P_{l,i} \delta \\
& \text{s.t.} \quad P_{s,i} + P_{\text{out},i} = P_{c,i} + P_{a,i} + P_{t,i} + P_{h,i} + P_{l,i} \\
& \quad P_{m,i} \geq \max\{P_{b,i}, \eta_b P_{b,i}\}, \\
& \quad E_i = E_{i-1} - \delta P_{m,i-1} \\
& \quad P_{b,i} \geq \frac{U_{\text{oc}}^2}{2R} \left(1 - \sqrt{1 - \frac{4R}{U_{\text{oc}}^2} P_{\text{out},i}} \right) \\
& \quad T_{c,i} = a_i (P_{c,i} + P_{h,i} + G_b T_{b,i} + G_f T_{f,i}) + b_i \\
& \quad P_{\text{out},i} \leq U_{\text{oc}}^2 / 4R \\
& \quad 0 \leq P_{h,i} \leq \bar{P}_h, \quad 0 \leq P_{l,i} \leq \bar{P}_l \\
& \quad \underline{T}_c \leq T_{c,i} \leq \bar{T}_c \\
& \quad \underline{E} \leq E_i \leq \bar{E}.
\end{aligned} \tag{75}$$

The first time-step of the solution of this problem defines the energy management strategy at the k th sampling instant and the process is repeated for each $k = 0, 1, \dots$ to define an MPC law. The procedure is summarised in Algorithm 1.

Algorithm 1: Energy management algorithm

```

 $k \leftarrow 0$ 
while True do
    Initialise the prediction horizon as follows
     $\mathbf{r}_{a,0}^{cg} \leftarrow \mathbf{r}_a^{cg}(k\delta)$ ,  $\mathbf{v}_{a,0}^{cg} \leftarrow \mathbf{v}_a^{cg}(k\delta)$ ,  $\omega_{b,0}^{ba} \leftarrow \omega_b^{ba}(k\delta)$ ,  $\omega_{b,0}^{wb} \leftarrow \omega_b^{wb}(k\delta)$ ,  $C_{ba,0} \leftarrow C_{ba}(k\delta)$ ,  $E_0 \leftarrow E(k\delta)$ ,
     $T_{b,0} \leftarrow T_b(k\delta)$ ,  $T_{s,0} \leftarrow T_s(k\delta)$ ,  $T_{c,0} \leftarrow T_c(k\delta)$ .
    for  $i \leftarrow 0$  to  $N-1$  do
        | Compute (47)-(74).
    end
    Compute the solution,  $\theta^* = (P_{\text{out}}^*, E^*, T_c^*, P_m^*, P_b^*, P_h^*, P_l^*)$ , of the OOCp (75).
    Implement the first element of this solution as follows
     $P_{\text{out}}(k\delta) \leftarrow P_{\text{out}}^*(0)$ ,  $E(k\delta) \leftarrow E^*(0)$ ,  $P_m(k\delta) \leftarrow P_m^*(0)$ ,  $P_b(k\delta) \leftarrow P_b^*(0)$ ,  $P_h(k\delta) \leftarrow P_h^*(0)$ ,  $P_l(k\delta) \leftarrow P_l^*(0)$ .
    Set  $k \leftarrow k+1$ 
end

```

4. Numerical results

4.1. Simulation scenario

We consider a vehicle inspired by the Eutelsat 172B, with parameters presented in Table 1. The convex OOCp (75) was specified using the general purpose convex optimisation package CVX using solver Mosek with a sampling interval $\delta = 50$ s and a prediction horizon of one orbit ($T = 24$ hours). The horizon size of the problem to be solved at each discrete time step k is thus $N = 1728$.

4.2. Discussion

The simulation results for 3 successive orbits are presented in Fig. 9. When the spacecraft is eclipsed by the Earth or when the incidence angle of the solar panel approaches 90° , solar power drops and the battery alone has to deliver the power required to accomplish the primary tasks. During eclipses, the temperature of the spacecraft drops and so does the temperature of the electronics, and therefore the heater has to provide enough power to keep the electronics temperature above its lower limit. This is only possible if enough energy is stored in the battery, thus requiring the spacecraft to accumulate solar energy in the battery during the illumination phase of the orbit. However, storing too much energy or charging the battery to its maximum would be overly conservative. Instead, in order to maximise the power available to secondary tasks,

Algorithm 1 anticipates future power demand and ensures that only the required amount of energy is stored. The limits on decision variables in the OOCp (75) are shown by red dashed lines in Fig. 9. From this it can be seen that the set of parameters chosen for this case study ensures that each of the inequality constraints of the OOCp become active at some point during the mission, and none are violated. This is a decisive advantage of MPC over heuristic energy management strategies that do not guarantee constraint satisfaction.

It is easy to modify the optimisation problem to allow more energy to be stored in case of contingency or unplanned events. Also, if continuity of the power available to the secondary task is important, it is possible to introduce a term \dot{P}_l in the objective so as to minimise volatility and avoid rapid variations during eclipses that are observed in Fig. 9.

Fig. 10 shows the residuals of inequalities (41) and (42), demonstrating that these are satisfied with equality (to the specified tolerance, namely $\epsilon = 1 \times 10^{-4}$) at the optimal solution.

4.3. Computational load

Fig. 11 shows the average time required to solve problem (75) as a function of prediction horizon size N on a MacBook Pro with a 2.9 GHz dual-core Intel Core i7 processor (mid-2012). For example, with a time step of $\delta = 50$ s and a horizon of one orbit, the prediction horizon consists of $N = 1728$ steps, and the average time to solve (75) is about

2 s. This suggests that real-time implementation is possible on modern embedded systems for sufficiently large time steps. Moreover, as shown in [12], solution time can be reduced significantly with first-order solvers such as the alternating direction method of multipliers (ADMM), allowing to solve the problem in real-time at higher sampling frequencies.

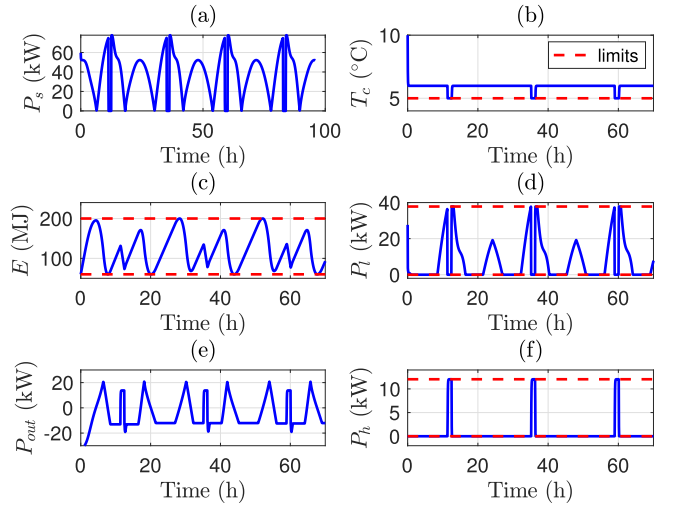
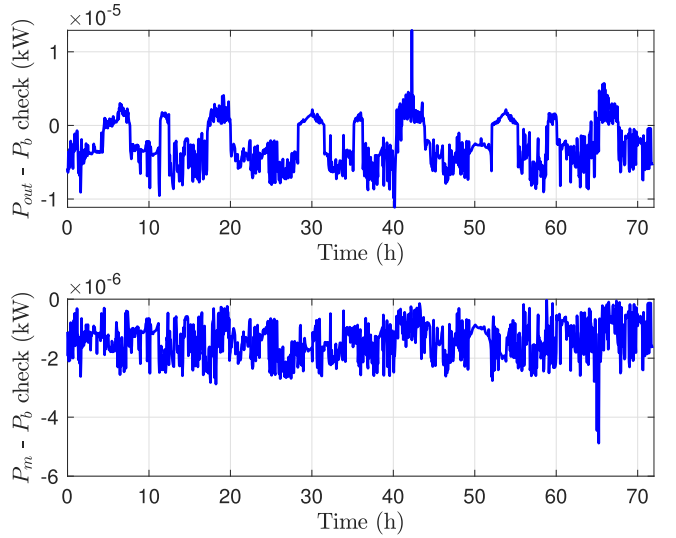
Another important aspect related to convergence is the choice of the horizon size N . The intuition is that for periodic problems, a receding horizon of one period is sufficient to capture all future information and is thus equivalent to solving the problem with an infinite horizon. A mathematical argument is given in the Appendix.

4.4. Robustness to parameter uncertainty

This section investigates the inherent robustness of the MPC strategy of Algorithm 1 to model errors. We consider two scenarios: first the case of uncertainty in model parameters in which the charging efficiency η is not known exactly, and second the case of structural uncertainty in the model in which the battery parameters U_{oc} and R depend on the battery state of charge according to a relationship that is unknown to the controller. In each case we simulate the closed-loop response of the MPC law that is derived from OOCp (75) with an inexact model. To emphasise the benefits of feedback we also show the results of applying the open loop control strategy that is obtained by solving the OOCp with an inexact model at the first time step ($k = 0$) only.

Table 1
Parameters.

Variable	Symbol	Value	Units
Time step	δ	50	s
Horizon size	N	1728	-
Total moment of inertia of spacecraft	J_b	diag{11778, 11778, 5122.5}	kg m ²
Moment of inertia of reaction wheels	\bar{J}_b	diag{22.5, 22.5, 22.5}	kg m ²
Solar array span	l_s	39	m
Total mass of spacecraft	m	3551	kg
Standard gravitational parameter of the Earth	μ	3.98×10^{14}	m ³ s ⁻²
Initial position	$r_{a,0}^{cg}$	$[-4.21 \times 10^4 \ 0 \ 0]^T$	km
Initial velocity	$v_{a,0}^{cg}$	$[0 \ 3.06 \ 0]^T$	km s ⁻¹
Initial angular velocity	$\omega_{b,0}^{ba}$	$[0 \ 0 \ 0]^T$	rad s ⁻¹
Initial attitude (DCM)	$C_{ba,0}$	diag{1, 1, 1}	-
Initial angular velocity of reaction wheels	$\omega_{b,0}^{wa}$	$[0 \ 0 \ 0]^T$	rad s ⁻¹
Battery resistance	R	0.067	Ω
Battery open-circuit voltage	U_{oc}	100.8	V
Electronics temperature range	$[T_c, \bar{T}_c]$	[5, 15]	°C
Electronics heat capacity	C_c	$1.74 \times 10^{+5}$	J K ⁻¹
Thermal conductance electronics/ surface	G_b	228	W K ⁻¹
Thermal conductance electronics/ heat pipe	G_f	2562	W K ⁻¹
Heat pipe fluid temperature	T_f	0	°C
Stefan-Boltzmann constant	σ	5.67×10^{-8}	W m ⁻² K ⁻⁴
Surface heat capacity	C_b	$5.5 \times 10^{+04}$	J K ⁻¹
Surface emissivity	ϵ_b	0.81	-
Surface area	S_b	17.10	m ²
Solar irradiation at Sun surface	G_0	$6.33 \times 10^{+7}$	W m ⁻²
Solar pressure (GEO orbit)	p	4.5×10^{-6}	N m ⁻²
Radius of the Sun	R_\odot	$6.96 \times 10^{+5}$	km
Radius of the Earth	R_\oplus	$6.37 \times 10^{+3}$	km
Astronomical Unit	AU	$1.5 \times 10^{+8}$	km
Surface solar absorptance	γ_b	0.87	-
Solar array solar absorptance	γ_s	0.50	-
Solar array heat capacity	C_s	$8.7 \times 10^{+4}$	J K ⁻¹
Solar array emissivity	ϵ_s	0.85	-
Solar array calibration parameter	I_0	4.38×10^{-04}	-
Solar array efficiency	η_s	0.95	-
Area of solar array	A_s	108.00	m ²
Solar array open-circuit voltage at $T_0 = 28^\circ\text{C}$	$V_{oc}(T_0)$	200	V
Solar array short-circuit current at $T_0 = 28^\circ\text{C}$	$I_{sc}(T_0)$	245.5	A
Solar array voltage thermal coefficient	$\alpha_{V_{oc}}$	-0.4650	V K ⁻¹
Solar array current thermal coefficient	$\beta_{I_{sc}}$	0.1440	A K ⁻¹
Boltzmann constant	k_B	1.380649×10^{-23}	m ² kg s ⁻² K ⁻¹
Electronics initial temperature	$T_{c,0}$	11.7	°C
Surface initial temperature	$T_{b,0}$	100	°C
Solar array initial temperature	$T_{s,0}$	-39	°C
Battery charging efficiency	η_b	0.7	-
Battery energy range	$[\underline{E}, \bar{E}]$	[66.5, 200]	MJ
Motor torque constant	k_a	2.6×10^{-04}	A N ⁻¹ m
Motor back emf constant	k_w	2.6×10^{-04}	V s rad ⁻¹
Motor armature resistance	R_a	1	Ω
HET Voltage	V_{HET}	100	V
HET Efficiency	η_{HET}	0.6	-
Average charge of Xe	\bar{q}	1.92×10^{-19}	C
Atomic mass of Xe	M	2.18×10^{-25}	kg
Maximum heater power	\bar{P}_h	$1.2 \times 10^{+4}$	W
Maximum load power	\bar{P}_l	$3.78 \times 10^{+4}$	W

**Fig. 9.** Simulation results. From (a) to (f): solar array power, temperature of the electronics, battery stored energy, power available for secondary tasks, battery output power, heater power.**Fig. 10.** Residuals of inequalities (41) and (42).

To investigate the effects of parametric uncertainty, we suppose that the charging efficiency η is underestimated or overestimated. This parameter appears in the OOCp via the inequality constraint (42), and an incorrect value directly affects the accuracy of predictions of the future battery energy state. The battery state of charge was updated using the true efficiency $\eta = 0.7$ in simulations, but the charging efficiency employed in the OOCp (75) ranged from $\eta = 0.4$ to $\eta = 0.8$. All other parameters are defined as in Table 1.

The evolution of the battery energy E over one orbit is shown in Fig. 12 for the MPC law (solid lines) and for the open loop application of the initial OOCp solution (dotted lines). The MPC strategy was able to adapt to the parametric uncertainty and therefore satisfied constraints for all η values between 0.4 and 0.8. On the other hand the open loop strategy violated the constraints whenever the charging efficiency η was not equal to the true value of 0.7.

To ensure a convex optimisation problem, the battery parameters U_{oc}, R are assumed to be constant in the OOCp (75). However, in practice these parameters usually depend on the battery state of charge. Fig. 13

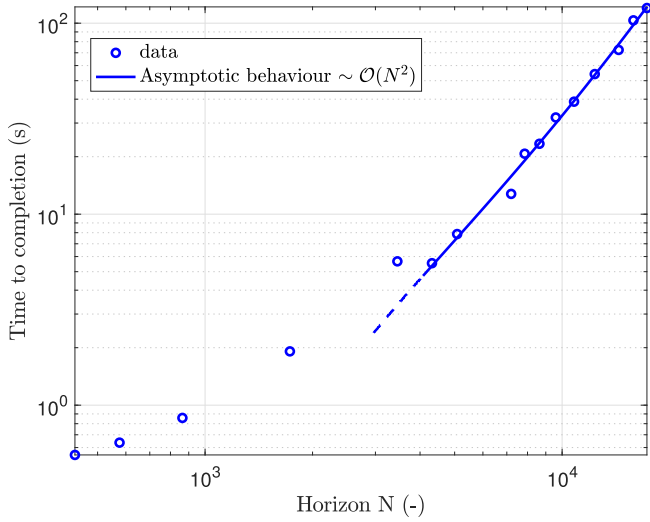


Fig. 11. Average time required to solve problem (75) as a function of horizon length. The estimated asymptotic complexity is quadratic with respect to N ($\sim \mathcal{O}(N^2)$).

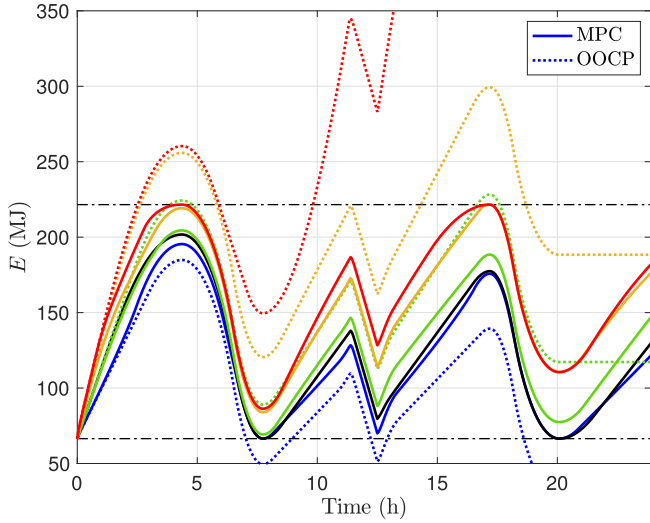


Fig. 12. The effect on battery stored energy (E) of uncertainty in battery charging efficiency η . Solid lines: MPC (Alg. 1). Dotted lines: open loop application of OOC solution at $k = 0$. Values of $\eta = 0.4, 0.5, 0.6, 0.7, 0.8$ in the OOC correspond to red, brown, green, black and blue lines respectively.

shows a set of open circuit voltage and internal resistance measurements obtained from a Li-ion battery together with approximate cubic polynomial relationships obtained via least squares (red lines) after scaling to match the batteries used in this simulation study. The effects of the model error introduced by neglecting the state of charge dependence in these parameters are shown in Fig. 14 for MPC and for the open loop application of the initial OOC solution. In both cases the values of U_{oc} and R were frozen at their current values when solving the OOC, whereas simulation updates were performed using U_{oc} and R that depend on the state of charge according to the cubic polynomials identified in Fig. 13. Clearly the MPC strategy is able to cope with the model uncertainty, and its response is almost identical to that of MPC with an exact model. On the other hand, since the initial OOC solution was computed with a small value of E , it has underestimated the value of U_{oc} over most of the prediction horizon, causing the battery to overcharge when applied in open-loop.

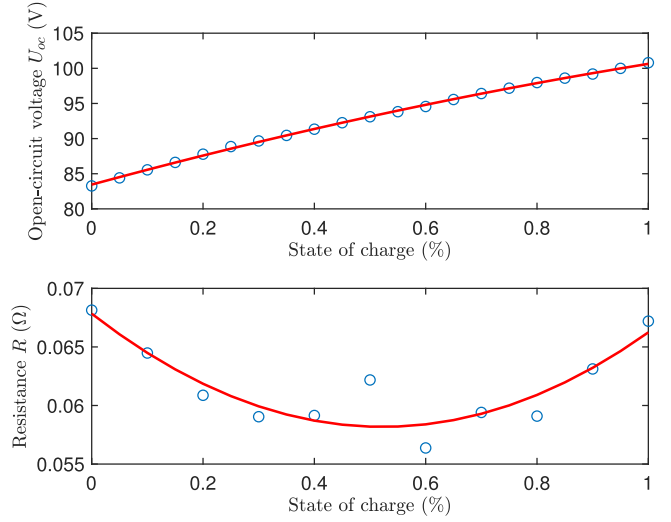


Fig. 13. The dependence of the battery open circuit voltage U_{oc} and internal resistance R on state of charge.

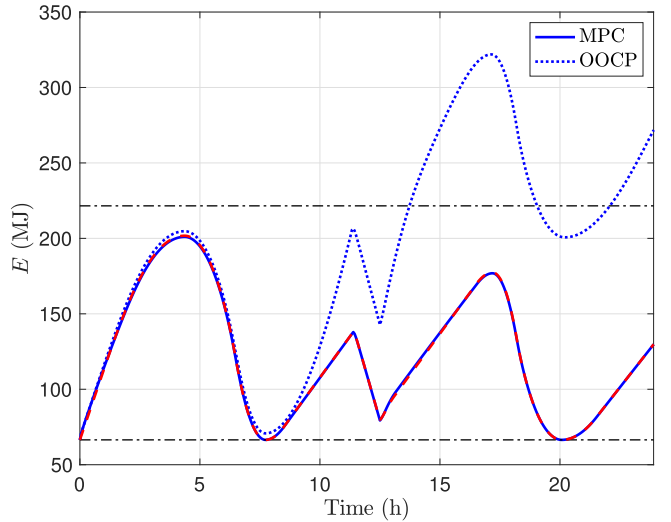


Fig. 14. The effect on battery stored energy (E) of uncertainty in the dependence of battery open-circuit voltage and resistance (U_{oc}, R) on state of charge. Solid line: MPC. Dotted line: open-loop application of the initial OOC solution. Dashed red line: MPC for the case of no model uncertainty.

5. Conclusions

This paper proposes a MPC strategy for spacecraft energy management based on the principle of maximising the power available to secondary tasks while meeting the demand for primary tasks and satisfying constraints on power flow and energy storage capacity. The optimisation problem is made tractable by a convex reformulation of the derived mathematical models. The main contribution of this research is a computationally tractable, fully-automated, model-based, optimal energy management strategy for spacecraft missions that require the power allocation among the different subsystems to be scheduled subject to operating constraints. Another contribution is to show that convex optimisation can be leveraged to solve energy management problems in realistic scenarios involving multiphysics subsystems. The convex nature of the problem also offers theoretical guarantees of convergence to a global optimum, provided a feasible solution exists.

A direct extension of this work is to develop first-order solvers (such as ADMM or fast gradient descent), which have better scalability if low-

or medium-accuracy solutions are required, and greater potential for parallelisation. Another extension is to consider different power sources and storage devices (e.g. fuel cells, nuclear power plant, super-capacitors) and to extend the presented models accordingly. Different optimisation objectives could be investigated, such as minimising battery ageing or minimising thermal stresses on components. Other mission scenarios could also be explored, such as telecommunication missions where a trade-off has to be made between pointing towards the Earth and pointing at the Sun to generate solar power, or low-earth-orbit missions where eclipse duration is longer or interplanetary missions.

Future work will include aspects of the vehicle position and attitude as optimisation variables and use reaction wheels both for control and kinetic energy storage. Finally, the framework presented could be modified by allowing component parameters to become optimisation

variables, thus providing a method of optimal system design.

CRedit authorship contribution statement

Martin Doff-Sotta: Conceptualization, Methodology, Software, Validation, Investigation. **Mark Cannon:** Conceptualization, Methodology, Software, Validation, Supervision, Project administration. **James Richard Forbes:** Conceptualization, Resources, Supervision.

Declaration of Competing Interest

The authors declare that they have no known competing financial interests or personal relationships that could have appeared to influence the work reported in this paper.

Appendix A

We show that using a finite horizon of one orbit is equivalent to using an infinite horizon for problem (75).

Theorem 1. Consider the following constrained optimisation problem with an infinite horizon

$$\min_{\theta} \sum_{i=0}^{\infty} \theta_i, \quad \text{s.t. } \theta \in \mathcal{C}, \quad \dagger$$

where θ is a N -periodic optimisation variable, i.e. $\theta_i = \theta_{i+kN}$ for all integers i, k and \mathcal{C} is a non-empty constraint set. Problem (\dagger) is equivalent to the following finite-horizon problem

$$\min_{\theta} \sum_{i=0}^{N-1} \theta_i, \quad \text{s.t. } \theta \in \mathcal{C}, \quad \ddagger$$

where $\theta_i = \theta_{i+kN}$, for all integers i, k .

Proof. The objective of problem (\dagger) can be rewritten as $\lim_{M \rightarrow \infty} \sum_{i=0}^M \theta_i = \lim_{M \rightarrow \infty} \sum_{k=0}^M \sum_{i=kN}^{(k+1)N-1} \theta_i$. Since $\theta_i = \theta_{i+kN}$, for all i, k , the sum $\sum_{i=kN}^{(k+1)N-1} \theta_i$ yields the same result for an arbitrary value of k . In particular, evaluating the sum for $k = 0$, the objective can be expressed as $\lim_{M \rightarrow \infty} \sum_{k=0}^M \sum_{i=0}^{N-1} \theta_i = \lim_{M \rightarrow \infty} M \sum_{i=0}^{N-1} \theta_i$, which is equivalent to the objective of problem (\ddagger) . \square

Finally, the following results show that Theorem 1 is applicable to the problem considered in this paper.

Lemma 1. Let f_1, f_2 be N_1 - and N_2 -periodic functions. Then, the function $f_1 + f_2$ is $\text{lcm}\{N_1, N_2\}$ -periodic where $\text{lcm}\{N_1, N_2\}$ is the least common multiple of N_1 and N_2 .

Theorem 2. The discretised variable P_i in optimisation problem (75) is (at least) N -periodic.

Proof. We note first that the discretised variables P_s, P_a and P_t are N -periodic functions since they depend on the orbital position of the vehicle. From Eq. (1), and using Lemma 1, we conclude that P_i has a periodicity that is a divisor of N . \square

References

- [1] Saleh JH, Geng F, Ku M, Walker II ML. Electric propulsion reliability: Statistical analysis of on-orbit anomalies and comparative analysis of electric versus chemical propulsion failure rates. *Acta Astronautica* 2017;139:141–56.
- [2] Rovey JL, Lyne CT, Mundahl AJ, Rasmont N, Glascock MS, Wainwright MJ, Berg SP. Review of multimode space propulsion. *Prog Aerospace Sci* 2020;118.
- [3] Chen Q, Liu Z, Zhang X, Zhu L. *Spacecraft Power System Technologies*. Springer; 2020.
- [4] Gluck PR. Spacecraft power management software for the new millennium. In: *IECEC-97 Proceedings of the Thirty-Second Intersociety Energy Conversion Engineering Conference* (Cat. No. 97CH6203), vol. 4. IEEE; 1997. pp. 2228–2230.
- [5] Soeder JF, Mcnelis A, Beach R, Mcnelis N, Dever T, Trase L, May R. Overview of intelligent power controller development for human deep space exploration. In: *12th International Energy Conversion Engineering Conference*; 2014. p. 3833.
- [6] Lee J, Kim E, Shin KG. Design and management of satellite power systems. In: *2013 IEEE 34th Real-Time Systems Symposium*. IEEE; 2013. p. 97–106.
- [7] Han J, Wang C, Zhao G, Huang Y. Research on braking energy recovery and energy management system for spacecraft. In: *2014 IEEE Conference and Expo Transportation Electrification Asia-Pacific (ITEC Asia-Pacific)*. IEEE; 2014. p. 1–5.
- [8] Yoshihara H, Takahashi M. Optimal power management considering attitude control and battery deterioration control for spacecraft with vsmg/ipacs. In: *AIAA SciTech 2020 Forum*; 2020. p. 1200.
- [9] Posielek T. An energy management approach for satellites. In: *Proceedings of the International Astronautical Congress, IAC*; 2018.
- [10] East S, Cannon M. Energy management in plug-in hybrid electric vehicles: Convex optimization algorithms for model predictive control. *IEEE Trans Control Syst Technol* 2020;28(6):2191–203.
- [11] Doff-Sotta M, Cannon M, Bacic M. Optimal energy management for hybrid electric aircraft. *IFAC*; 2020.
- [12] Doff-Sotta M, Cannon M, Bacic M. Predictive energy management for hybrid electric aircraft propulsion systems. *arXiv preprint arXiv:2103.07909*; 2021.
- [13] East S, Cannon M. Scenario model predictive control for data-based energy management in plug-in hybrid electric vehicles. *IEEE Trans Control Syst Technol* (Early Access) 2022. <https://doi.org/10.1109/TCST.2022.3154155>.
- [14] Boyd S, Boyd SP, Vandenberghe L. *Convex optimization*. Cambridge University Press; 2004.
- [15] Kouvaritakis B, Cannon M. *Model predictive control*, vol. 38. Switzerland: Springer International Publishing; 2016.
- [16] Grant M, Boyd S. Graph implementations for nonsmooth convex programs. In: *Recent Advances in Learning and Control* (V. Blondel, S. Boyd, and H. Kimura, eds.), *Lecture Notes in Control and Information Sciences*, Springer-Verlag Limited; 2008. pp. 95–110.
- [17] ApS M. *The MOSEK optimization toolbox for MATLAB manual*. Version 9.0 2019.
- [18] Larson WJ, Wertz JR. *Space mission analysis and design*. Torrance, CA (United States): Microcosm Inc; 1992. tech. rep..
- [19] De Ruiter AH, Damaren C, Forbes JR. *Spacecraft dynamics and control: an introduction*. John Wiley & Sons; 2012.
- [20] Bate RR, Mueller DD, White JE, Saylor WW. *Fundamentals of astrodynamics*. Dover; 2020.

- [21] Hughes PC. Spacecraft attitude dynamics. Dover; 2004.
- [22] Longo CRO. Method for the calculation of spacecraft umbra and penumbra shadow terminator points. National Aeronautics and Space Administration 1995;vol. 3547.
- [23] Guzzella L, Sciarretta A, et al. Vehicle propulsion systems, vol. 1. Springer; 2007.
- [24] Goebel DM, Katz I. Fundamentals of electric propulsion: ion and Hall thrusters, vol. 1. John Wiley & Sons; 2008.
- [25] Lee T, Leok M, McClamroch NH. Geometric tracking control of a quadrotor UAV on SE(3). In: 49th IEEE conference on decision and control (CDC). IEEE; 2010. p. 5420–5.
- [26] Patel MR. Spacecraft power systems. CRC Press; 2004.
- [27] Patel MR. Wind and solar power systems; 2009.
- [28] Tian H, Mancilla-David F, Ellis K, Muljadi E, Jenkins P. A cell-to-module-to-array detailed model for photovoltaic panels. Solar Energy 2012;86(9):2695–706.
- [29] Corless RM, Gonnet GH, Hare DE, Jeffrey DJ, Knuth DE. On the Lambert W function. Adv Comput Math 1996;5(1):329–59.
- [30] Barry D, Parlange J-Y, Li L, Prommer H, Cunningham C, Stagnitti F. Analytical approximations for real values of the Lambert W function. Math Comput Simul 2000;53(1–2):95–103.
- [31] Silk E. Introduction to spacecraft thermal design, vol. 48. Cambridge University Press; 2020.